Anal. Bioanal. Electrochem., Vol. 17, No. 2, 2025, 173-189
https://www.doi.org/10.22034/abec.2025.721575

Analytical & Bioanalytical Electrochemistry

Full Paper

Electrochemical Study of the Interaction Between Urea and Hydroquinone, and Detection of Urea Using $CoFe_2O_4$ Nanoparticles Modified with Gelatin-Hydroquinone Deposited on the Glassy Carbon Electrode

Moussa Djerafa,[1,2] Mosbah Ferkhi,[1,2,*] Ebru Kuyumcu Savan,[3] and Smail Khelili,[2,4]

[1]*Laboratory of Materials Interaction and Environment (LIME), Faculty of Exact Sciences and Computer Science, University of Jijel, 18000 Jijel, Algeria*
[2]*Department of Chemistry, Faculty of Exact Sciences and Computer Science, University of Jijel, 18000 Jijel, Algeria*
[3]*Division of Analytical Chemistry, Department of Basic Pharmaceutical Sciences, Faculty of Pharmacy, İnönü University, Malatya, Turkey*
[4]*Labotatory of pharmacology and phytochemistry, team of pharmaceutical chemistry and quality control of drugs, Faculty of Exact Sciences and Computer Science, University of Jijel, 18000 Jijel, Algeria*

*Corresponding Author, Tel.: +213670351700
E-Mail: ferkhi_m@univ-jijel.dz

Received: 17 November 2024 / Received in revised form: 2 February 2025 / Accepted: 14 February 2025 / Published online: 28 February 2025

Abstract- An advanced electrochemical biosensor has been developed to measure the amount of urea in biological fluids accurately using $CoFe_2O_4$ nanoparticles modified with Gelatin-hydroquinone deposited on the glassy carbon electrode. This sensor uses cobalt ferrite as a core material that has been analysed using X-ray diffraction (XRD) and scanning electron microscopy (SEM). The sensor has a Gelatin-hydroquinone layer that allows it to detect urea at trace levels. in this study, it has been confirmed that the electrochemical method using this modified electrode is significantly more sensitive than the UV-visible method. The limit of detection (LOD) obtained utilizing the modified Berthelot reaction was 6.66 mM, while the LOD obtained using CV at the CFO/Gelatin-hydroquinone modified GCE was 0.52 mM. This confirms that the electrochemical method using this modified electrode is significantly more sensitive than the UV-visible method. The CFO/Gelatin-hydroquinone composite material effectively acted as an efficient electrocatalyst for the oxidation of urea and other molecules.

Keywords- Urea; Hydroquinone; $CoFe_2O_4$ nanoparticles; XRD analysis; Electrochemical properties

1. INTRODUCTION

Urea, also recognized by its chemical moniker carbamide and represented by the molecular formula $CO(NH_2)_2$, is a byproduct of protein catabolism in humans. It serves a vital function in averting acidosis or ionic imbalance stemming from the presence of NH_4^+ [1]. Under typical physiological conditions, urea circulates within the bloodstream at concentrations fluctuating between 15 to 40 mg/dL (2.5–7.5 mM) [2]. The quantification of urea is of paramount importance in clinical diagnostics, as it serves as a primary indicator of the functional status of the liver and the kidneys, as well as a critical marker of the efficacity of hemodialysis treatments [3]. As known, the urea concentrations surpassing 6.7 mmol/L in blood and 333 mmol/L in urine are indicative of compromised kidney and liver functionality. Therefore, the development of a simplistic yet effective sensor for urea measurement has garnered immense research interest. Among various quantification techniques, electrochemical methods stand out due to their rapid operation, exceptional selectivity and sensitivity, and notably low detection thresholds [4,5]. For instance, electrodes incorporating cobalt-based electrocatalysts have been successfully implemented for urea detection [6,7]. Ferrite nanoparticles, typified by the formula MB_2O_4, where 'M' denotes a divalent metal like Cu^{2+}, Ni^{2+}, Zn^{2+}, Mn^{2+} and Co^{2+} [8]. They have garnered attention across a spectrum of applications, ranging from industrial to medical domains, owing to their pronounced anisotropy, resistance to oxidation, magnetic properties, chemical stability, and mechanical robustness [9,10]. Hydroquinone, a compound with widespread applications in industries like textiles, pharmaceuticals, dyes, oil refineries, and cosmetics [11,12], is paired with Gelatin; a natural polymer derived from the hydrolysis of collagen found in animal skin, bones, tendons, and ligaments [13,14]. This study presents the synthesis of cobalt ferrite ($CoFe_2O_4$), nanoparticles via the sol-gel citrate method, followed by the surface modification with Gelatin-hydroquinone. The functionalization process involved the use of glutaraldehyde to prepare the nanoparticle's surface for immobilization. Comprehensive characterization of the ferrite nanoparticles, both pre and post-modification, was conducted using XRD and SEM techniques. cyclic voltammetry (CV) and electrochemical impedance spectroscopy (EIS) were employed as electrochemical techniques. The findings have shown that the as-prepared ferrites adjusted with Gelatin-hydroquinone exhibited promising capabilities for urea detection, with a marked enhancement in peak current values in comparison to the unadopted ferrite nanoparticles.

2. EXPERIMENTAL SECTION

2.1. Chemicals and reagents

A suite of precursors including $Co(NO_3)_3{\cdot}6H_2O$ (≥ 99%), $Fe(NO_3).9H_2O$ (≥ 98%), citric acid ($C_6H_80_7/H_2O$) (≥ 98%), ferricyanide $K_3[Fe(CN)_6]$ and ferrocyanide $K_4[Fe(CN)_6]$ (≥ 99%), urea (≥ 99.5%), hydroquinone (≥ 99%), gluteraldehyde (25%), THF(C_4H_8O) (≥ 99.9%), were sourced from Biochem and Sigma. These analytical-grade reagents were used without additional purification. The preparation of all aqueous solution samples was meticulously

performed using de-ionized water to ensure the highest degree of purity and consistency in the experimental procedures.

2.2. Synthesis of CFO nanoparticles

The nanoparticles of cobalt ferrite ($CoFe_2O_4$**)** were crafted using a sol-gel citrate technique that is notably uncomplicated [15-19]. The primary inorganic precursors were solubilized in distilled water, combined, and then put on a heated plate. Citric acid was introduced as a chelating agent while the mixture was stirred at 75 to 85°C until it thickened into a gel. By escalating the temperature to 120°C, a fluffy black substance will be obtained and then reduced on powder. This resultant powder underwent a tiered heat treatment in a muffle furnace; initially at 300°C for one hour, followed by 500°C, and culminating at 850 C° for four hours to produce the final powder. The nanomaterial was thus readied for investigation.

2.3. Assembly of electrode

The modified electrode was produced through multiple steps. Firstly, the GCE was polished with 0.05 μm alumina powder and rinsed with ethanol to remove surface contaminants. Next, the GCE underwent CV in 0.1 M PBS at 150 mV/s for 20 cycles within a potential range of -0.8 to 1 V. Following this, the GCE surface was modified with $CoFe_2O_4$, by taking a volume of 5 μL of a mixture prepared by combining a minute quantity of $CoFe_2O_4$ (0.1 mg) with 1 milliliter of tetrahydrofuran (THF), which was then subjected to ultrasonication for 15 minutes. After that, the Gelatin-hydroquinone polymer was prepared by blending 2 mL of hydroquinone and 2 mL of Gelatin. The Gelatin-hydroquinone was attached to CFO/GCE by cross-linking method immersing the CFO/GCE in 2 mL of PBS with 5 μL of glutaraldehyde at 25% and 5 μL of Gelatin-hydroquinone polymer for 2h at room temperature. The resulting Gelatin-hydroquinone/CFO/GCE biosensor was then saved in PBS at 4°C for other analytical assays.

2.4. Electrochemical instrumentation, performance evaluation, and measurement techniques

Measurements of electrochemical experiments were conducted at room temperature using a Solartron potentiostat/galvanostat controlled by dedicated software. A three-electrode setup was employed, consisting of a modified glassy carbon electrode (GCE, 0.3 mm diameter) as the working electrode, a platinum (Pt) counter electrode, and a saturated calomel electrode (The SCE served as the reference electrode. Before measurement, the WE was immersed in the test solution at room temperature for 15 minutes to ensure a stable open-circuit potential and optimize urea adsorption. Subsequently, the potential was scanned from −0.4 V to +0.85 V (vs. SCE) at various scan rates in 0.1 mmol/L PBS (pH 7.0), containing urea concentrations ranging from 0.1 mg/mL to 1.5 mg/mL. Cyclic voltammetry (CV) was also used to determine the

electrode surface area in a solution of 3 mmol/L $[Fe(CN)_6]^{3-/4-}$ and 0.1 mmol/L PBS as the supporting electrolyte. EIS data were assembled over a frequency range from 10^5 to 10^{-2} Hz. All experiments were performed at 25°C [20].

3. RESULTS AND DISCUSSION

3.1. X-ray diffraction analysis (XRD)

Through XRD measurements and subsequent Rietveld refinement, as illustrated in Figure 1, the phase and structural properties of the synthesized cobalt ferrite nanoparticles (CFO) were confirmed. The XRD revealed a cubic structure for $CoFe_2O_4$, which aligns with the Fd3m space group, as verified by the Rietveld refinement process [2]. The structural parameters and the refinement process were conducted using the Jana 2006 software [20].

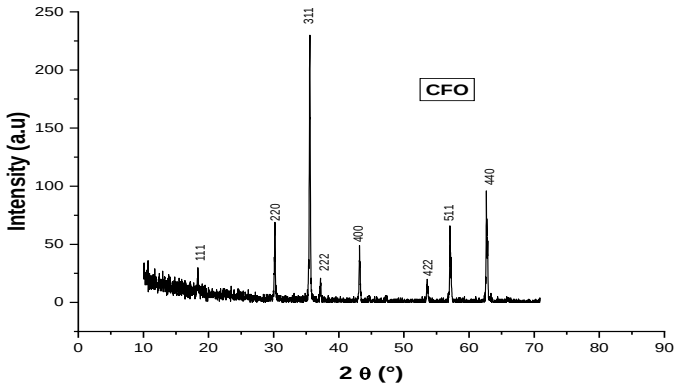

Figure 1. X-ray diffraction of the CFO powders

The XRD analysis revealed distinct peaks for the crystal planes (111), (220), (311), (222), (400), (422), (511), and (440) planes were obtained at 18.3°, 30.22°, 35.5°, 37.26°, 43.14°, 53.69°, 57.21°, and 62.55° (JCPDS card no. 22–1086) for pure $CoFe_2O_4$ [21-23]. The lack of additional peaks suggests that the nanomaterials prepared are highly pure and crystalline. Scherrer's equation yielded a mean crystallite size for the $CoFe_2O_4$ phase of 50.31 nm [23]. The lattice constant measured from the XRD analysis was 0.836592 nm as shown in Table 1, which verifies the spinel structure in the sample being analyzed which is very similar to the results of anterior studies [24,25].

Table 1. Crystallographic parameters of the synthesized CFO nano-particles

Materials	**Lattice parameters (S.G) a=b=c**	**α = β = γ**	**Volume (Å3)**	**References**
CFO	8.37 (A°)	90°	585.52	This work
$CoFe_2O_4$	8.26 (A°)	90°	563.56	[24]
CFO	8.37(A°)	90°	586.97	[25]

3.2. Scanning electron microscopy analysis (SEM)

The FE-SEM analysis explored the morphological features of the pure $CoFe_2O_4$. The synthesized $CoFe_2O_4$ nanoparticles as depicted in Figure 2, exhibit an agglomerate-like nanosheet morphology [26]. The electrode's structure revealed porosity, along with well-defined crystallinity and a uniform distribution [27]. Additionally, the material demonstrates multiscale porosity, which enhances its electrocatalytic performance for increasing the specific surface area [28,29] and thereby enhancing the diffusion of urea through the modified electrode's pores over a period of five seconds. Additionally, the material exhibits multiscale porosity, which enhances its electrocatalytic performance by increasing the specific surface area [28,29] and thereby promoting the diffusion of urea through the electrode pores.

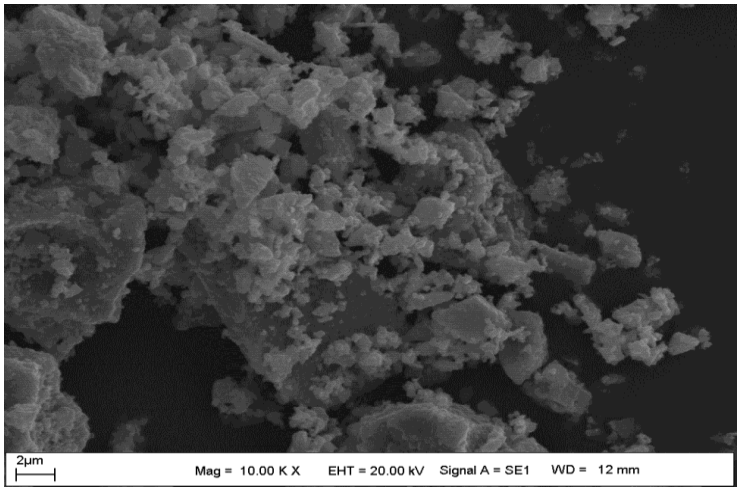

Figure 2. SEM image of CFO nanomaterial (scale bar = 2 µm)

3.3. Electrochemical investigation of CFO and CFO/Gelatin-hydroquinone modified electrodes for urea detection

3.3.1. Ferro-cyanide test

The electron transfer behavior of the redox couple at CFO/GCE was studied using CV. The potential was range from -0.4 to +0.85 V (*vs.* SCE) in a 3 mM $[Fe(CN)_6]^{3-/4-}$ solution in PBS. Scan rates varied from 5 to 75 mV/s. The results in Figure 3a revealed an increase in redox peaks current I_p (both anodic (I_{pa}) and cathodic (I_{pc}) peaks) with higher scan rates for the CFO/GCE electrode. At 50 mV/s, the anodic-to-cathodic current ratio was approximately 1, indicating good redox reversibility. Additionally, the peak separation potential (ΔE=0.36 V) increased due to positive shifts in anodic peak potential and negative shifts in cathodic peak potential with increasing scan rate, confirming a reversible process at the electrode surface [30].

To understand the reaction mechanism of both diffusion or adsorption-controlled, oxidation-reduction mechanisms and kinetic parameters, cyclic voltammograms of

$[Fe(CN)_6]^{3-/4-}$ were evaluated at different scan rates, from 5 to 75 mV, on the same modified GCE surface (supporting information of Figure 3a [31]). The peak current for anodic oxidation followed a square root dependence on the scan rate. The linear regression equation for this relationship is $I_{pa} = 3.92488.10^{-6} + 2.79885.10^{-6}\ v^{1/2}$ ($R^2 = 0.99703$) and $I_{pc} = -1.32557.10^{-6} – 1.83428.10^{-6}\ v^{1/2}$ ($R^2 = 0.99651$).

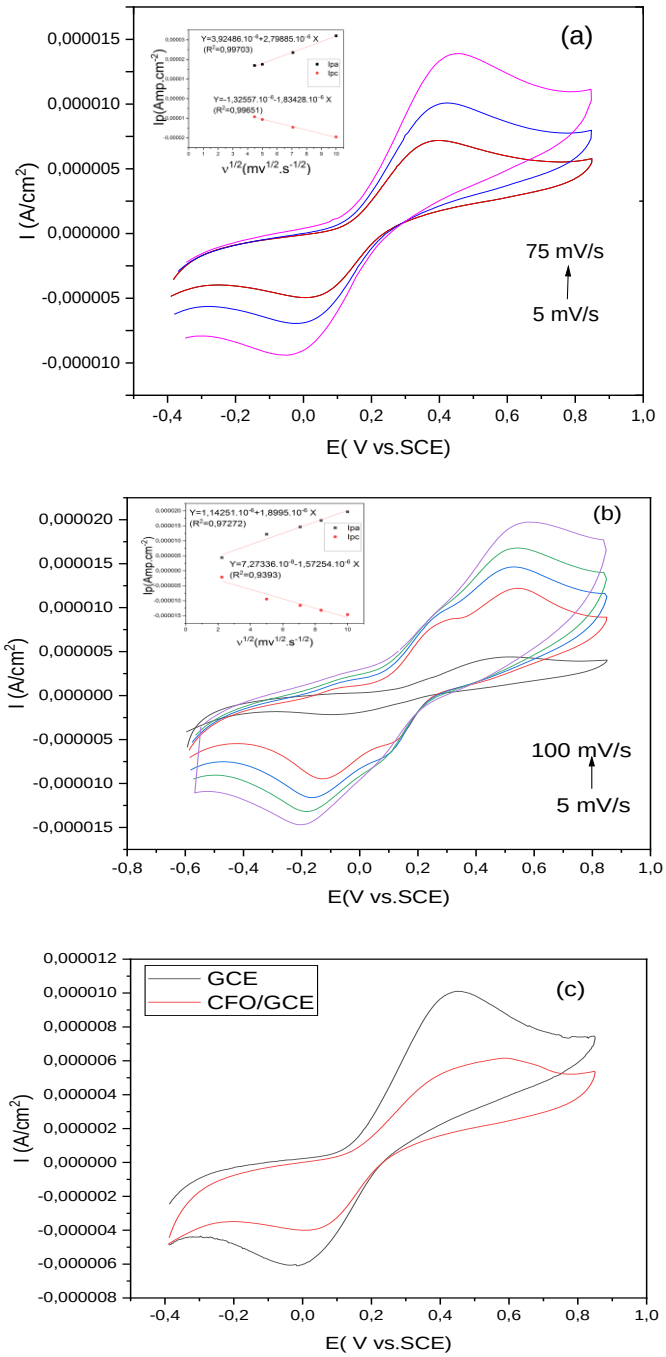

Figure 3. (a) Cyclic voltammograms plots corresponding to $[Fe(CN)_6]^{4-}/[Fe(CN)_6]^{3-}$ mixture at 3 mM for CFO deposited on GCE at different scan rates from 5 to 75 mVs^{-1}, in 0.1 mM PBS at pH 7.0 and its Linear plot of I_{pa} and I_{pc} of $[Fe(CN)_6]^{4-}/[Fe(CN)_6]^{3-}$ vs $(\text{scan rate})^{1/2}$; (b) Cyclic voltammogram plots corresponding to 3 mM $[Fe(CN)_6]^{4-}/[Fe(CN)_6]^{3-}$ mixture at modified GCE

with Gelatin. Hydroquinone at different scan rates. And its linear plots of I_p *vs.* (scan rate)$^{1/2}$; (c) The electron-transfer capabilities of electrodes at each modification step in containing 3 mM $[Fe(CN)_6]^{3-/4-}$ PBS solution (pH = 7.0) using CV at the scan-rate of 25 mV s^{-1}

According to the Randles-Sevcik formula [32], the peak current (Ip) can be obtained using the equation $I_p=2.69\times105.n^{3/2}ACD^{1/2}v^{1/2}$ where n represents the number of electrons transferred, A is the surface area of the electrode, C is the concentration of electroactive species, D is the diffusion coefficient, and v denotes the scan rate of the potential. The findings suggest that the electrochemical reactions at the electrodes are governed by diffusion [33,34]. Moreover, CV was employed to examine the comportment of various modified electrodes. A comparative analysis of the CV curves was performed for the GCE and CFO-modified GCE electrode at a fixed scan rate of 25 mV/s in 3 mM $[Fe(CN)_6]^{3-/4-}$ in PBS solution with a pH of 7.0 revealing a distinct pair of redox peaks. Figure 3c presents a comparative analysis of the cyclic voltammograms recorded at both the bare GCE and the CFO/GCE at a scan rate of 25 mV/s in 3 mM $[Fe(CN)_6]^{3-/4-}$ (PBS, pH 7.0). The unmodified GCE displays distinct redox peaks corresponding to the reversible redox behavior of the ferricyanide ion. After modification of the GCE with CFO using THF, the cathodic and anodic peak currents decrease slightly, primarily due to a blocking effect from the THF head, although the high conductivity of CFO still promotes electron transfer. These results confirm the successful fabrication of the CFO/GCE electrode [35]. Subsequently, the CV response of varying scan rates on the GCE modified with CFO/Gelatin-hydroquinone was examined. This study utilized 3 mM $[Fe(CN)_6]^{3-/4-}$ solution in PBS, with scan rates from 5 mV/s to 100 mV/s as shown in Figure 3 b. The unmodified GCE displayed peak oxidation at 0.52 V, and it was observed that both the oxidation and reduction peak currents increased linearly with the square root of the scan rate. The calibration plots for I_{pa} *vs.* $v^{1/2}$ and I_{pc} *vs.* $v^{1/2}$, $I_{pa} = 1.14251.10^{-6} + 1.89695.10^{-6}\ v^{1/2}$ (R^2 = 0.97272) and $I_{pc} = 7.27336.10^{-6} - 1.57254.10^{-6}\ v^{1/2}$ (R^2 = 0.9393) demonstrated excellent linear relationships, indicating that the electrochemical reactions on the modified GCE were diffusion-controlled events - with a peak around 0.28 V likely due to impurities [36].

3.3.2. Urea Detection by Cyclic Voltammetry in PBS

3.3.2.1. Voltammetric behavior of urea at GCE modified with CFO

Cyclic voltammograms were carried out at scan rates ranging from 5 to 150 mV/s to investigate the urea response on the CFO/GCE sensor surface. Increasing the scan rate led to higher peak currents, with an oxidation peak appearing around 0.28 V. Notably, at 100 mV/s, the oxidation peak was nearly absent on the bare GCE; however, beyond 25 mV/s, the peak became increasingly prominent with higher scan rates (Figure 4b). These observations suggest that urea in PBS undergoes irreversible reaction kinetics at both electrodes [37].

3.3.2.2. Voltammetric behavior of urea at GCE modified with CFO/Gelatin-hydroquinone

Typically, phenolic compound is electro-oxidized to quinones by proton transfer reactions [38]. The electrochemical performance of the fabricated electrodes was assessed by using CV in the presence of hydroquinone [35]. For this reason, an electrocatalytic performance of the CFO/GCE electrode toward HQ was examined through cyclic voltammetry (CV).

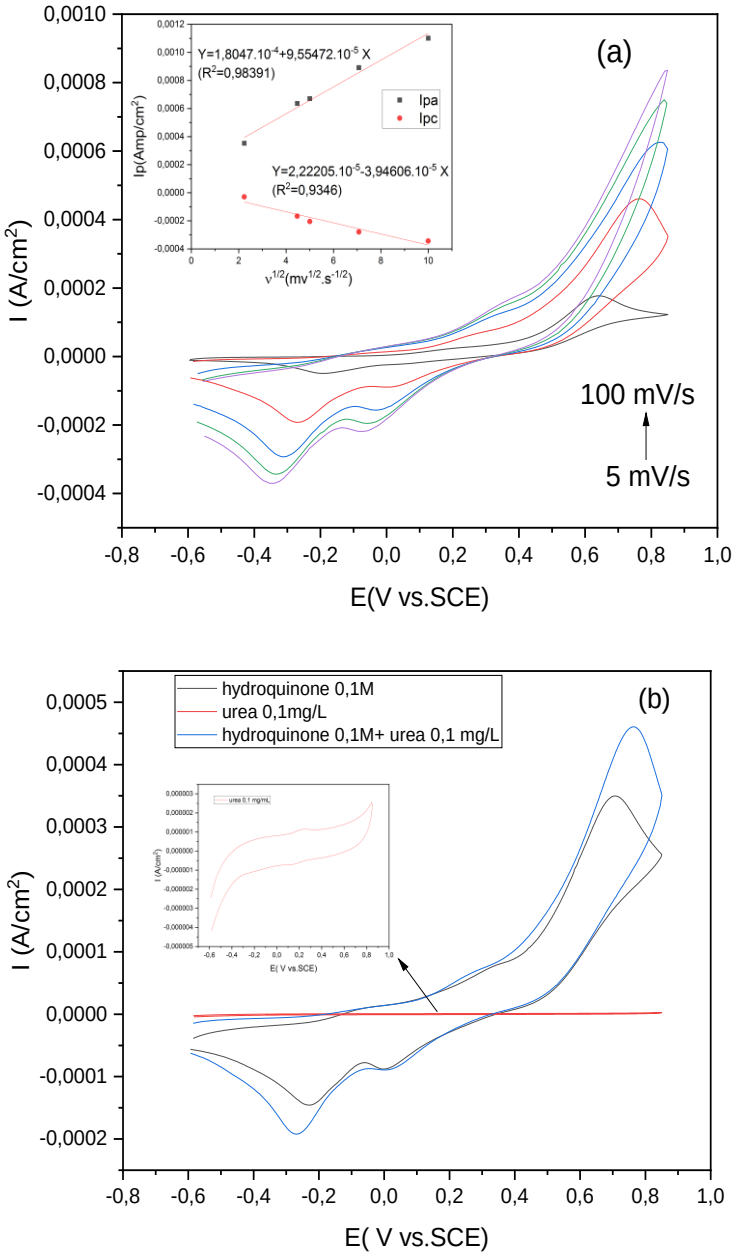

Figure 4. (a) The electron behavior of 0.1 M hydroquinone at the modified GCE/CFO using cyclic voltammetric technique vs different scan rates Linear plot of I_{pa} of hydroquinone at GCE/CFO *vs.* different scan rates; (b) Comparison of cyclic voltammograms relating to the solutions: 1.66 mM of [urea], 0.1 M hydroquinone, and a mixture of 0.1 M hydroquinone and 1.66 mM of urea at 25 mV/s scan rate

Figure 4a presents the cyclic voltammetric response of the CFO/GCE-modified electrode in a pH 7.0 solution containing 0.1 M HQ, recorded at scan rates ranging from 5 to 100 mV/s. The CFO/GCE modified electrode exhibited an electrochemical response in the potential range between 0.01 V to 0.74 V due to the oxidation and reduction of HQ/Q. This suggests that the CFO/GCE modified electrode is electrochemically active in pH 7.0 within the specific potential range, while a peak around -0.22 V appeared due to impurities. It is necessary to mention the peak current of the oxidation of hydroquinone and reduction of quinone at 25 mV/s 6.39×10^{-4} and -1.6×10^{-4} A/cm^2 respectively.

The influence of scan rate on the electrochemical redox behavior of HQ at the CFO/GCE-modified electrode was examined using cyclic voltammetry. Figure 4a shows the CV response of the CFO/GCE modified electrode at pH 7.0 containing 0.1 M HQ and at scan rates varying between 5-100 mV/s. It was observed that both anodic and cathodic peak currents of HQ increase with higher scan rates. Moreover, plotting the square root of the scan rate against the corresponding peak currents reveals a linear correlation within the range of 5–100 mV/s, indicating that the anodic and cathodic peak currents of HQ are proportional to the square root of the scan rate. The linear regression equations for anodic and cathodic peak currents versus the square root of scan rate are $I_{pa}=1.8047.10^{-4} + 9.55472.10^{-5}v^{1/2}$ ($R^2 = 0.98391$) and $I_{pc}= 2.22205.10^{-5}-3.94606.10^{-5}v^{1/2}$ ($R^2 = 0.9346$) respectively. This observation confirms that the electrochemical response of HQ at the CFO/GCE-modified electrode follows a diffusion-controlled process [39]. The mechanism of hydroquinone oxidation is illustrated in the equation below [40].

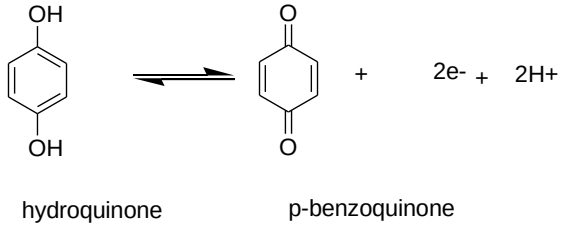

Scheme 1. Mechanism of hydroquinone oxidation

To explore the interaction between urea and hydroquinone, we conducted a comparative study at the modified electrode with a scan rate of 25 mV/s. Figure 4b illustrates the results when only hydroquinone (0.1 M) was present, two peaks corresponding to HQ/Q oxidation and reduction were observed. However, in the presence of urea, these peaks showed reduced current intensity, suggesting an interaction between the two molecules. CV serves as a highly sensitive technique commonly employed for electrochemical detection. In Figure 5a, CV curves were observed for various urea concentrations on a CFO/Gelatin-hydroquinone-modified GCE.

Notably, the electro-catalytic oxidation peak current of hydroquinone exhibits a linear decrease with increasing urea concentration (ranging from 6.66 to 16.65 mM). Figure 5a demonstrates a strong linear correlation between the concentrations and peak currents with a linear correlation coefficient (R^2 = 0.99339). This finding underscores the high sensitivity and urea-dependent behavior of hydroquinone oxidation at the CFO/Gelatin-hydroquinone-modified electrode surface. This study involved three replicates, giving reproducible results. Previously researchers have synthesized various nanomaterials to develop electrochemical sensors for urea detection [41-43].

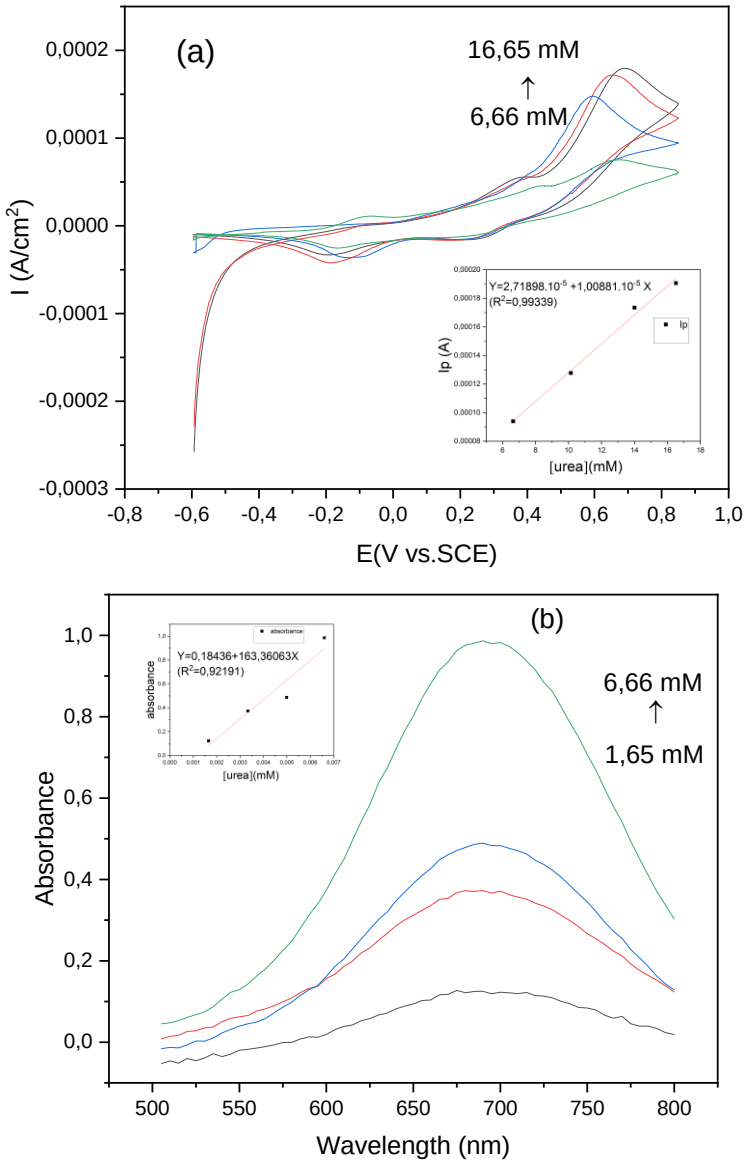

Figure 5. (a) CV of CFO/Gelatin-hydroquinone modified GCE recorded over urea concentrations range from 6.66 to 16.65 mM. and its calibration curve of urea (I_{pa} *vs.* [Urea]); (b) UV-visible spectrum of urea samples varying from 500-800 nm wavelength; (b) inset, UV-visible calibration curve of urea (Absorbance *vs.* [urea]) at ⅄=695 nm)

Additionally, the analytical data in this study was compared with other reported urea detection methods (Table 1). This proposed approach offers several advantages, including a linear detector response range (6.65-16.65 mg/mL) comparable to existing methods. Furthermore, it demonstrates improved selectivity and a lower limit of detection (LOD) for urea (Table 2). The LOD was calculated by the bellow Equation:

$$LOD = 3\sigma/S \qquad \text{Eq. (1)}$$

Here σ, represents the standard deviation of current measured on a blank sample (4.59927×10^{-5} A) and S is the slope of the calibration curve (2.60416×10^{-4} A mM^{-1}A). The resulting LOD value (0.52 mM) outperforms some previously reported urea sensors (Table 2).

Table 2. Examples of direct urea electrochemical sensors and their analytical performances

Materials	Electroanalytical Method	Linearity Range (M)	Detection Limit (M)	References
$NiCo_2O_4$/NNs/GCE	CV	1×10^{-5}–5×10^{-3}	1.0×10^{-6}	[53]
Urs-Nafion-MWCNT- PANI-Fe_3O_4-GCE	CV, DPV, CA	1.0×10^{-3}-2.5×10^{-2}	6.7×10^{-5}	[54]
Urs-ZnO-MWCNT-ITO	CV	1.6×10^{-3}-1.6×10^{-2}	2.3×10^{-4}	[55]
CFO/Gelatin-Hydroquinone/ GCE	CV	6.7×10^{-3} –16.7×10^{-3}	5.2×10^{-4}	This study

3.4. Electrochemical impedance spectroscopy

The EIS was used to identify and analyze the contributions and properties of the electrolyte and electrode [44]. Electrochemical measurements concentrate on the processes occurring at the electrode surface. It is well-established that higher electrolyte concentrations result in reduced measured resistance [45]. Furthermore, research indicates that working with more conductive solutions can enhance the theoretical fit of an electrochemical spectrum [46-48]. Therefore, increasing concentration could improve system accuracy and reliability.

The obtained EIS measurements were conducted at 25°C using a 10 mL volume with varying urea concentrations in PBS (pH = 7.4) via a Voltalab Potentiostat-Galvanostat. The frequency was scanned from 10^{-2} to 100 kHz with an amplitude of 10 mV. An open circuit potential (OCP) of 0.22 V was applied to the cell. To assess the impact of redox probe

concentration on the electrochemical response, we varied urea concentration from 0.1 to 50 mg/mL using bare gold electrodes (Figure 6).

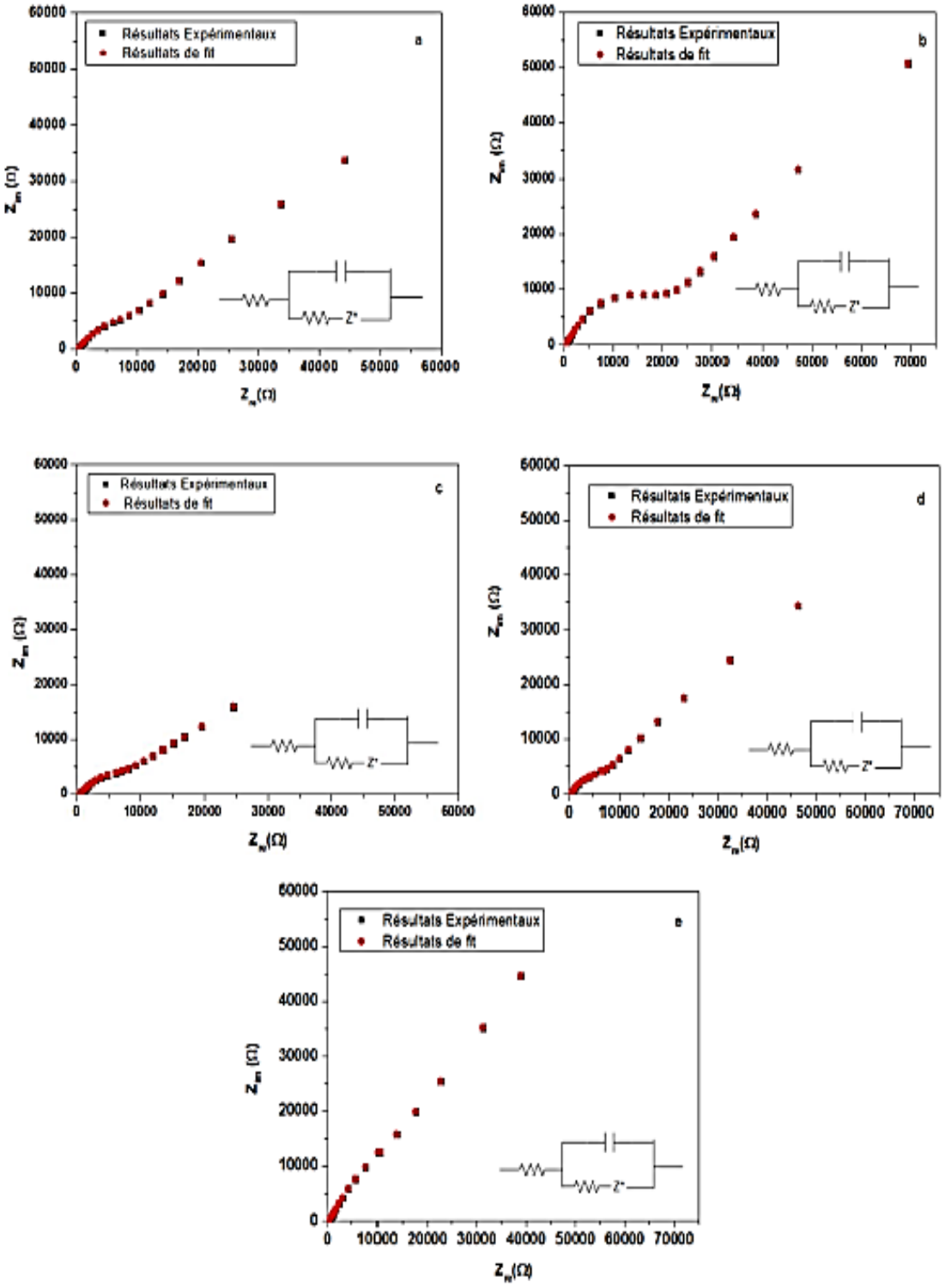

Figure 6. Experimental and simulation Nyquist diagrams for CFO/Gelatin-hydroquinone electrocatalysts: (a) 1.66 mM; (b) 8.32 mM; c) 16.65 mM; d) 499.5 mM; and e) 832.5 mM with their fits in 10^5 to 10^{-1} Hz frequency domains

The EC-Lab program is utilized for Zft analysis of all Nyquist plots [49] and shown in Figure 6. As the concentration increases, resistance behavior becomes more pronounced. Figure 6 reveals the following principal regions derived from fitting each concentration diagram:

(a) At frequencies above 10^5 Hz (R_1), the observed response corresponds to the electrolyte resistance; (b) in the range of 10^5 to 10^{-1} Hz (R_2), a semicircle appears, indicative of charge transfer between the electrode and the electrolyte; (c) below 10^{-1} Hz (R_3), another semicircle reflects the adsorption and diffusion of urea molecules on the WE surface [50].

3.5. Comparison with UV-visible method

Serum electrolyte levels (Na^+, K^+, and Cl^-) were measured by colorimetric methods, following the protocols of Maruna (1958), Trinder (1951), Terri and Sesin (1958), and Skeggs and Hochstrasser (1964), respectively. Serum bicarbonate was determined using the back-titration method described by Van Slyke et al. (1919). Serum urea and creatinine were quantified using the Urease-Berthelot method (Berthelot, 1859) and the Jaffe reaction (Bonsnes and Taussky, 1945), respectively [51,52]. Urease catalyzes the hydrolysis of urea into ammonia and carbamic acid, which rapidly decompose to yield carbon dioxide and an additional ammonia molecule. The liberated ammonia subsequently reacts with water to form ammonium hydroxide.

In the urea-modified Berthelot reaction, the ammonium ions generated in an alkaline medium react with hypochlorite and salicylate (substituting for phenol), under the catalytic action of nitroprusside, to produce indophenol with a characteristic blue-green color. The reaction sequence, in which salicylate replaces the aromatic compound, is shown below [52].

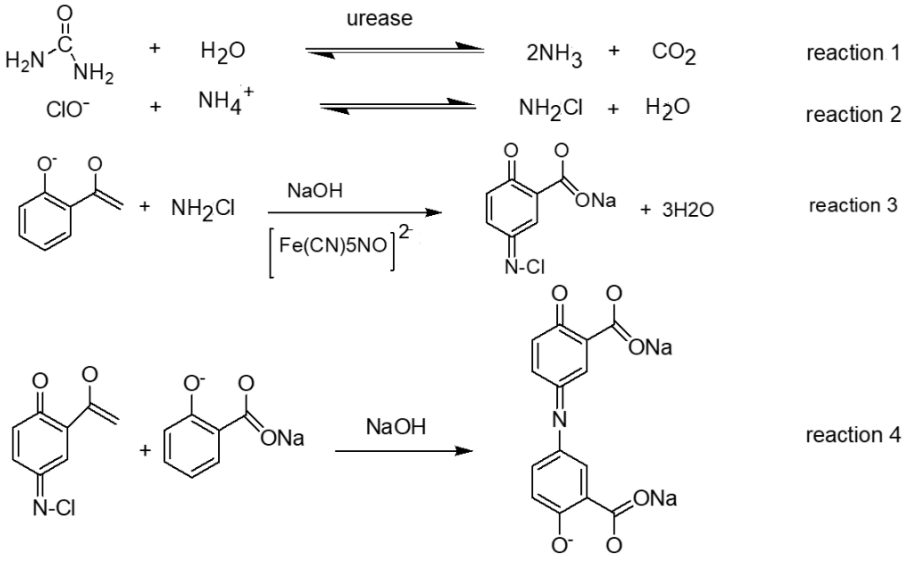

The sample preparation involves a two-step using two reagents. Firstly, 1000 µL of reagent 1 (containing phosphate buffer at 120 mmol/L, EDTA at 1 mmol/L, sodium salicylate at 60

mmol/L, sodium nitroprusside at 5 mmol/L, and urease at 5 kU/L) is mixed with 10 µL of urea solution and incubated for 5 minutes at 25 °C. In the second step, the resulting solution is combined with 1000 µL of reagent 2 (containing sodium hypochlorite at 10 mmol/L, sodium hydroxide at 400 mmol/L, and phosphate buffer at 120 mmol/L) and incubated for 10 minutes at 25°C. The resulting solution turns green, as shown in Figure 5b. The UV spectrum of urea concentrations ranging from 1.65 mM to 6.66 mM was investigated at wavelengths from 500 to 800 nm to understand urea's behavior. It was observed that there is a higher absorbance at 695 nm. The absorbance versus urea concentration plot demonstrates a clear linear relationship at a wavelength of 695 nm. The precise linear regression equation for absorbance versus concentration is absorbance = 0.18436+163.36063C (R^2=0.92191) (Figure 5b). The limit of detection (LOD) obtained utilizing the modified Berthelot reaction was 6.66 mM, while the LOD obtained using CV at the CFO/Gelatin-hydroquinone modified GCE was 0.52 mM. This confirms that the electrochemical method using this modified electrode is significantly more sensitive than the UV-visible method.

4. CONCLUSION

The preparation of the GCE with CFO nanocomposite was carried out efficiently, resulting in a robust and electrochemically stable electrode. In comparison to the bar electrode, the constructed nanocomposite electrode exhibited significantly enhanced electrocatalytic performance for urea detection. Notably, the oxidation peaks at CFO/Gelatin-hydroquinone-modified electrodes displayed well-defined oxidation peaks of hydroquinone in the presence of urea. These peaks exhibited a pronounced separation, a reduced oxidation potential, and higher oxidation currents. The composite material allowed for good linear ranges by CV determination of urea, with lower detection limits than those reported in the literature. In summary, the CFO/Gelatin–hydroquinone composite exhibited strong detection performance for the oxidation of urea.

Acknowledgments

Part of this work was prepared in collaboration with the Laboratory of Electrochemistry and Materials (LEM).

Declarations of interest

The authors declare that they have no known competing financial interests or personal relationships that could have appeared to influence the work reported in this paper.

Data availability

No data was used for the research described in the article.

REFERENCES

[1] J. H¨aberle, N. Boddaert, A. Burlina, A. Chakrapani, M. Dixon, M. Huemer, D. Karall, D. Martinelli, P. Crespo, R. Santer, A. Servais, V. Valayannopoulos, M. Lindner, V. Rubio, and C. Dionisi-Vici, Orphanet J. Rare Dis. 7 (2012) 32.

[2] S.N. Botewad, D.K. Gaikwad, N.B. Girhe, H.N. Thorat, and P.P. Pawar, Biotechnol. Appl. Biochem. (2021) 1.

[3] L. Quadrini, S. Laschi, C. Ciccone, F. Catelani, and I. Palchetti, Trends Anal. Chem. 168 (2023)117345.

[4] N.S. Arun Kumar, P.S. Adarakatti, S. Ashoka, and P. Malingappa, J. Solid State Electrochem. 22 (2018) 1711.

[5] X. Zhu, B. Liu, H. Hou, Z. Huang, K.M. Zeinu, L. Huang, X. Yuan, D. Guo, J. Hu, and J. Yang, Electrochim. Acta 248 (2017) 46.

[6] P. Salarizadeh, M.B. Askari, N. Askari, and N. Salarizadeh, Mater. Chem. Phys. 239 (2020) 121958.

[7] P. Basumatary, U.H. Lee, D. Konwar, and Y.S. Yoon, Int. J. Hydrogen Energy 45 (2020) 32770

[8] P.A. Vinosha, A. Manikandan, A.C. Preetha, A. Dinesh, Y. Slimani, M.A. Almessiere, A. Baykal, B. Xavier, and G. Nirmala, J. Supercond. Novel Magn. 34 (2021) 995.

[9] S.R. Mokhosi, W. Mdlalose, A. Nhlapo, and M. Singh, Pharmaceutics 14 (2022) 937.

[10] K.K. Kefeni, T.A.M. Msagati, and B.B. Mamba, Mater. Sci. Eng. B 215 (2017) 37.

[11] J. Ahmed, M.M. Rahman, I.A. Siddiquey, A.M. Asiri, and M.A. Hasnat, Sens Actuators, B 256 (2018) 383.

[12] S. Zheng, N. Zhang, L. Li, T. Liu, Y. Zhang, J. Tang, J. Guo, and S. Su, Sensors 23 (2023) 6957.

[13] J.A. Rather, N. Akhter, Q.S. Ashraf, S.A. Mir, H.A. Makroo, D. Majid, F.J. Barba, A. M. Khaneghah, and B.N. Dar, Food Package. Shelf Life 34 (2022) 100945.

[14] D.S. Liu, M. Nikoo, G. Boran, and P. Zhou, Annu. Rev. Food Sci. Technol. 6 (2015) 527.

[15] S. Amira, M. Ferkhi, A. Khaled, F. Mauvy, J.M. Bassat, M. Cassir, and J.C. Grenier, Mater. Res. Bull. (2023) 112400.

[16] S. Amira, M. Ferkhi, A. Khaled, and J.J. Pireaux, J. Iran. Chem. Soc. (2022) 1.

[17] M. Ferkhi, M. Rekaik, A. Khaled, M. Cassir, and J.J. Pireaux, Electrochim. Acta 229 (2017) 281.

[18] M. Ferkhi, and H.A. Yahia, Mater. Res. Bull. 83 (2016) 268.

[19] S. Amira, M. Ferkhi, F. Mauvy, S. Fourcade, J.M. Bassat, and J.C. Grenier, Electrocatalysis (2023) 1.

[20] M. Mekersi, M. Ferkhi, and E.K. Savan, Microchem. J 194 (2023) 109346.

[21] E.A. Chavarriaga, A.A. Lopera, V. Franco, C.P. Bergmann, and J. Alarcon, J. Magn. Magn. Mater. 497 (2020) 166054 .

[22] X. Feng, Y. Huang, X. Chen, C. Wei, X. Zhang, and M. Chen, J. Mater. Sci. 53 (2018) 2648.

[23] M. Ganesan, B. Ganapathi, P. Govindasamy, B. Parasuraman, P. Shanmugam, R. Boddula, R. Pothu, P. Thangavelu, Results Chem. 7 (2024) 101342.

[24] D.A. Larasati, D.L. Puspitarum, M.Y. Darmawan, N.I. Istiqomah, J. Partini, H. Aliah, E. Suharyadi, Results Mater. 19 (2023) 100431.

[25] Z. Jiang, L. Feng, and J. Zhu, Ceram Int. 47 (2021) 18140.

[26] H. Parangusan, J. Bhadra, K. Karuppasamy, T. Maiyalagan, Z. Ahmad, N. Al-Thani, Electrochim. Acta 464 (2023)142849.

[27] M. Ferkhi, A. Ringuedé , A. Khaled, L. Zerroual, and M. Cassir. Electrochim. Acta 75 (2012) 80.

[28] S. Amira, M. Ferkhi, M. Belghobsi, A. Khaled, F. Mauvy, and J.C. Grenier, Ionics 25 (2019) 3799.

[29] S. Amira, M. Ferkhi, A. Khaled, F. Mauvy, J.C. Grenier, L. Houssiau, and J.J. Pireaux, Ionics 25 (2019) 3809.

[30] Allen. J. Bard, and L.R. Faulkner, Electrochemical Methods Fundamentals and Applications, Wiley, New York (2001).

[31] E. Kuyumcu Savan, Anal. Lett. 53 (2019) 858.

[32] J. Wang, Analytical Electrochemistry, 3rd ed., Wiley-VCH, New Jersey (2006).

[33] A. Zine, M. Ferkhi, A. Khaled, and E.K. Savan, Electrocatalysis 13 (2022) 524.

[34] R.S. Nicholson, and I. Shain, Adv. Anal. Chem. Instrum. 36 (1964) 706.

[35] T. Ghosh, P. Sarkar, and A.P.F. Turner, Bioelectrochemistry 102 (2015) 1.

[36] S. Aini Hasnawati Ta'alia, E. Rohaeti, B.Riza Putra, and W. Tri Wahyuni, Results Chem. 6 (2023) 101024.

[37] E. Kuyumcu Savan, I. Ozcan, and S. Koytepe, Measurments 203 (2023)111979.

[38] F. Momeni, S.M. Khoshfetrat, and K. Zarei, ACS Appl. Nano Mater. 6 (2023) 19239.

[39] R. Madhu, S. Palanisamy, S.M. Chen, and S. Piraman, J. Electroanal. Chem. 727 (2014) 84.

[40] H. Nur Amirah Mustafa, I. Md Isa, N. Mohd Ali, N. Hashim, M. Musa, S. Ab Ghani, Int. J. Electrochem. Sci. 10 (2015) 9232.

[41] C. Wang, J. Li, K. Shi, Q. Wang, X. Zhao, Z. Xiong, X. Zou, and Y. Wang, J. Electroanal. Chem. 56 (2016) 770.

[42] E. de Pieri Troiani, and R.C. Faria, J. Appl. Electrochem. 43 (2013) 919.

[43] K.C. Lin, T.H. Tsai, and S.M. Chen, Biosens. Bioelectron. 26 (2010) 608.

[44] M. Ferkhi, S. Khelili, L. Zerroual , A. Ringuedé, and M. Cassir, Electrochim. Acta 54 (2009) 6341.

[45] M. Mekersi, M. Ferkhi, A. Khaled, N. Maouche, M. Foudia, and E.K. Savan, Surfaces and Interfaces 53 (2024) 104941.
[46] A. Lasia, Electrochemical Impedance Spectroscopy and its Applications. New York, NY: Springer New York (2014).
[47] L.L. Bridgewater, Standard methods for the examination of water and wastewater, American Public Health Association, Washington (2017).
[48] J.H. Sluyters, I. Theory, Recl. Trav. Chim. PaysBas 79 (1960) 1092.
[49] M. Mekersi, E.K. Savan, and M. Ferkhi, Ionics (2024) 1.
[50] R. Santos de Amorim, P.A. Serrano, G.E. Nunes, and I.H. Bechtold, Results in Chem. 7 (2024) 101488.
[51] A. Uchenna Emeribe, S. Obialor Anyanwu, I. Kokoabasi Isong, U. Remi Bassey, I. Joseph Inyang, E. Onyekachukwu Ibeneme, E. Aiyudubie Asemota, Z. Okhormhe, B. Icha, and I. Nasir Abdullahi, Saudi J. Biol. Sci. 28 (2021) 6748.
[52] W. Toito Suarez, B. Roberto de Alvarenga Junior, M. de Oliveira Krambeck Franco, W. Lira Gabriel, D. Mendes de Oliveira, and V. Bezerra dos Santos, Food Anal. Methods 3 (2016) 2719.
[53] S. Amin, A. Tahira, A. Solangi, V. Beni, J.R. Morante, X. Liu, M. Falhman, R. Mazzaro, Z.H. Ibupoto, and A. Vomiero, RSC Advances 9 (2019) 14443.
[54] A.K. Singh, M. Singh, and N. Verma, J. Food Meas. Char. 14 (2020) 163.
[55] M. Tak, V. Gupta, and M. Tomar, J. Mater. Chem. B 1 (2013) 6392.